Applied Catalysis B: Environmental 129 (2013) 301–308

Contents lists available at SciVerse ScienceDirect

Applied Catalysis B: Environmental

journal homepage: www.elsevier.com/locate/apcatb

Catalytic degradation of tobacco-specific nitrosamines by ferric zeolite

Wei Gang Lin[a], Yu Zhou[a], Fang Na Gu[a], Shi Lu Zhou[a,b], Jian Hua Zhu[a,*]

[a] Key Laboratory of Mesoscopic Chemistry of MOE, College of Chemistry and Chemical Engineering, Nanjing University, Nanjing 210093, China
[b] China Tobacco Shandong Industrial Co. Ltd., Tsinan 250000, China

ARTICLE INFO

Article history:
Received 31 May 2012
Received in revised form 6 September 2012
Accepted 22 September 2012
Available online 29 September 2012

Keywords:
Ferric zeolite
Tobacco-specific nitrosamines (TSNA)
Ion-exchange and impregnation
Catalytic degradation
Cigarette-catalyst (cig-cat)

ABSTRACT

New strategy of using ferric zeolite ZSM-5 and Y to adsorb and catalytically degrade tobacco-specific nitrosamines (TSNA) is reported in this article. These zeolites were modified by both aqueous ion-exchange with $FeSO_4$ solution and wet-impregnation of $Fe(NO_3)_3$, and characterized by XRD, UV–vis DRS, H_2-TPR and temperature-programmed surface reaction (TPSR). Apart from laboratory tests, these samples were put into tobacco rods of cigarette to assess their real performance of reducing TSNA content in smoke, and the determination of TSNA was carried out by LC–MS/MS technique with the assistance of internal-standards. The ion-exchanged zeolites are more active than their impregnated analogs, and the ferric Y zeolite could selectively reduce 26% of total TSNA in mainstream smoke of Burley type tobacco. Catalytic breaking of the chemical bond in N—NO group of nitrosamines by zeolite is the key step of decomposition of these carcinogens.

1. Introduction

No matter how often antismoking campaigns are shown, some people will never give up cigarette so that smoking is still a serious environmental problem in many countries. Among thousands of compounds in tobacco smoke, tobacco-specific nitrosamines (TSNA), consisting of N′-nitrosonornicotine (NNN), 4-methylnitrosarnino-1-3-pyridyl-1-butanone (NNK), N′-nitrosoanatabine (NAT), and N′-nitrosoanabasine (NAB), are the most active carcinogens [1,2]. A lot of efforts have been contributed to reduce these carcinogens level in smoke, and many investigations focused on utilizing molecular sieves to reduce the pollutants such as TSNA in smoke [3–10]. However, TSNA mostly exist in the particle phase of tobacco smoke and these particles have the size of micrometer grade [11,12], exceeding the pore diameter of common zeolites or mesoporous silica. Some new capturers, such as the SBA-15 with 3D net-like structure and CAS-1 with fiber-like morphology, could intercept the particles in smoke and thus reduce the TSNA content [7,8]; but it is hard, if not impossible, to selectively trap the carcinogen TSNA in smoke. Alternatively, how about adding catalyst directly into cigarette to try *in situ* degradation of TSNA? It sounds attractive that this strategy will simultaneously cut down the carcinogens both in mainstream and side stream smoke; but there are many suspicions: How the catalyst catches the TSNA in smoke and separates them from the particulate matter? How the additives catalyze the degradation of TSNA in the burning cigarette at the fluky temperature which changes so quickly? To answer these questions is important not only for controlling the environment carcinogenic pollutants, but also for developing selective catalysis in the extremely complex system.

Mesoporous silica possesses a well structural symmetry and large pore volume, but lacks the fine geometric confinement and active sites; so its catalytic performance for nitrosamine degradation is inferior to zeolites [4,9]. For this reason, zeolites have been chosen as the additives into cigarette to remove nitrosamines in smoke [5,6]. Consequently, we try to seek more efficient and cost-effective catalysts based on common zeolite candidates. Loading transition metal oxide such as copper and cobalt oxide on zeolites could obviously increase their affinity toward nitrosamine molecules [3,10]. However, the relative toxicity of copper and cobalt loaded zeolites limits their practical applications in environmental catalysis, which spurs us to seek new modifier for zeolite.

Ferric zeolite is the versatile catalysts for many environmental reactions including selective reduction of NO_x and selective oxidation of NH_3 to nitrogen, and it has been used for controlling automotive diesel emissions and waste steam of factory; also, it is an excellent catalyst for decomposition of harmful nitrous oxide such as N_2O [13–19]. Special interaction between ferric species and NO_x implies the possibility that ferric zeolite can be a competitive candidate for catalytic removal of TSNA in smoke, because all nitrosamines have the N—NO group that should also interact with the ferric species in the zeolite. Fe species can be introduced into zeolite by many methods, among them ion-exchange and wet-impregnation are common ones to form different Fe species, such as isolated ion, oligonuclear iron complex, FeO_x nanoparticles and large iron oxide particles [19]. However, questions remain here if

* Corresponding author. Tel.: +86 25 83595848; fax: +86 25 83317761.
E-mail address: jhzhu@netra.nju.edu.cn (J.H. Zhu).

0926-3373/$ – see front matter © 2012 Elsevier B.V. All rights reserved.
http://dx.doi.org/10.1016/j.apcatb.2012.09.039

we apply ferric zeolite to remove TSNA in smoke, that is, which form of ferric species plays the major role in nitrosamine degradation? Does the catalyst performing well in laboratory tests also present a high efficiency in smoke? Thus, we will evaluate the zeolite both in laboratorial experiments and in tobacco smoke. NaZSM-5 and NaY zeolites were modified by ferric species through both aqueous ion-exchange and wet-impregnation method, and their catalytic activity was assessed with temperature-programmed surface reaction (TPSR) in laboratory. Moreover, these catalysts were put into tobacco rods of cigarette to reduce the TSNA content of smoke; and the liquid chromatography–tandem mass spectrometry (LC–MS/MS) was employed with deuterated TSNA as the internal standard substance to determine the TSNA content of smoke [20].

2. Experimental

2.1. Materials

NPYR (*N*-nitrosopyrrolidine) and NNN (*N*′-nitrosonornicotine) were purchased from Sigma. Zeolite NaZSM-5 and NaY are commercially available powder samples [3]. The purity of N_2 and H_2 gases was 99.99%, and all other agents used here were of A.R. grade. Burley type tobacco and cigarette pipe were provided by Etsong Tobacco Group (China).

Ferric zeolites were prepared by two methods. One was aqueous ion-exchange [21,22]: 4 g zeolite was added into 120 mL $FeSO_4$ solution with a certain concentration, and stirred at 323 K for 20 h under nitrogen atmosphere followed by filtering and washing. After calcination in air flow at 413 K for 1 h and then 823 K for 5 h with the heating rate of 1 K min^{-1}, the product was denoted as FeZ(x) for ZSM-5 and FeY(x) for Y zeolite where x indicates the initial concentration (M) of Fe^{2+} solution. Another preparation was wet-impregnation in which the calculated amount of $Fe(NO_3)_3$, according to Fe content detected in ion-exchanged samples, was dissolved in 40 mL deionized water and then 5 g zeolite was added. The suspension was stirred at room temperature for 2 h and evaporated at 353 K with stirring until dryness. The obtained solid sample was calcined as mentioned above.

To prepare the sample cigarette containing zeolite additive, 750 mg Burley type fine cut tobacco and 30 mg powder zeolite were mixed manually in an agate until homogeneousness, and then hand-made to cigarette by use of commercial cigarette pipe with filter tip. These hand-made cigarettes were carefully selected to ensure their error of weight and pressure drop below ±2% and ±5%, respectively. For comparison, the control cigarette was prepared in same procedure without addition of zeolite. Both the sample and the control cigarettes were conditioned for at least 48 h at 295 K and 60% relative humidity (R.H.) before smoking tests.

2.2. Measurements

X-ray diffraction (XRD) patterns were recorded on an ARL XTRA diffractometer with Cu K_α radiation [3]. Nitrogen adsorption of sample at 77 K was measured on a Micromeritics ASAP 2020 volumetric adsorption analyzer, and the sample was outgassed at 573 K before measurements. The BET specific surface area was calculated using adsorption data acquired at a relative pressure (p/p_0) range of 0.05–0.22 and the total pore volume determined from the amount adsorbed at a relative pressure of 0.99, both with error below 3%. The chemical composition of sample was detected by X-ray fluorescence (XRF) method using ARL-9800 X-ray fluorescence spectrometer. UV–vis diffuse-reflectance spectra (UV–vis DRS) were obtained on a Shimadzu UV-2550 spectrophotometer adapted with a DR praying-mantis accessory using $BaSO_4$ as a standard. Temperature-programmed reduction with H_2 (H_2-TPR) was carried out on Quantachrome Automated chemisorption analyzer (chemBET pulsar TPR/TPD) [4], and 100 mg granular sample (20–40 mesh) was pretreated in an Ar stream at 573 K for 0.5 h.

TPSR (temperature-programmed surface reaction) test of NPYR or NNN was conducted as reported previously [9,23]. TG-DSC analysis of the used samples was performed to measure their coke contents formed in TPSR test [9]. A set of Netzsch STA449C TG/DSC-MS was utilized to analyze the decomposed products of NNN from 303 K to 773 K under Ar flow and the released components were sent to the mass spectrometer by carrier gas [23,24].

Ten cigarettes were smoked on a SM450 smoking machine (Borgwaldt) under ISO standard conditions (35 cm^3 puff, 2 s duration every 60 s), and the particulate phase of smoke was separated through a standard Cambridge filter pad [20]. The Cambridge filter pad was then added with 100 μL internal-standard (50 ng for each deuterated TSNA), and then extracted, further cleaned-up and analyzed by Agilent 6410 Triple Quad LC–MS/MS [8]. An Agilent 1200 LC system was used for chromatographic separation, and the quantification of each TSNA was performed by using internal standard method [20].

3. Results

3.1. Structure and composition of ferric zeolites

Table 1 lists the textural property and chemical composition of ferric zeolite. These samples kept same Si/Al ratio to their parent zeolites. For ion-exchanged ZSM-5 zeolite, the Fe^{2+} solution of 0.02 M had exchanged a large proportion of Na^+ ions in NaZSM-5 to reach the Fe/Al ratio of 0.225, near the calculated saturated value (0.33); hence the solution with a higher Fe^{2+} concentration (0.1 M) only increased this ratio (0.267) quarter larger on the sample FeZ(0.1). The Fe content of ion-exchanged Y zeolite strongly depended on the Fe^{2+} concentration of solution: FeY(0.02) sample had a relative low Fe/Al ratio of 0.095 while FeY(0.1) elevated this ratio to 0.24. Ion-exchanged samples possessed a comparative or slightly lower surface area and pore volume than their parents; the decreased extent became higher as the Fe^{2+} concentration of ion-exchange solution increasing because some oligonuclear iron complex or nanoparticles formed [19]. Due to serious aggregation of ferric species, the impregnated samples had obviously lower surface area and pore volume than their ion-exchanged analogs.

Fig. S1 displays the wide-angle XRD patterns of ferric zeolites. Both ferric ZSM-5 and Y kept their original structure, but the peak intensity of ferric Y sample decreased as its Fe content increased, due to the enhanced absorption of X-ray by Fe cations [25–27]. Fig. S1B shows the magnified XRD patterns of ferric ZSM-5 samples, in which the peak of α-Fe_2O_3 was absent on FeZ(x) samples but slightly emerged in the pattern of 2.2%Fe_2O_3/NaZSM-5 at the 2θ of 33.2° and 35.7°. No crystalline phase was found on ferric Y zeolites no matter prepared by ion-exchange or wet-impregnation.

3.2. Adsorptive and catalytic activity in laboratory test

Table 2 demonstrates the adsorbed and degraded amounts of NPYR and NNN by different zeolites in TPSR process, and NPYR has the structure similar to NNN but the pyridine group is replaced by hydrogen molecule (Scheme S1). About 360–460 μmol g^{-1} of NPYR was adsorbed by these zeolites, depending on their Fe content and textural property. FeZ(0.1) sample trapped more NPYR (389 μmol g^{-1}) than NaZSM-5 (375 μmol g^{-1}) though its surface area was reduced by about 8%. Similarly, more NPYR (425 μmol g^{-1}) was adsorbed by FeY(0.1) than NaY (407 μmol g^{-1}) despite the former had the 23% smaller surface area. Higher

Table 1
Relevant parameters of ferric zeolites and their parents.

Sample	Si/Al	Na/Al	Fe/Al	Surface area ($m^2\ g^{-1}$)	Pore size (nm)	Pore volume ($cm^3\ g^{-1}$)	H_2/Fe^a
NaZSM-5	12.0	1.05	0	306	0.54 × 0.56	0.168	–
FeZ(0.02)	12.1	0.29	0.225	327		0.171	0.69
FeZ(0.1)	12.0	0.23	0.267	279		0.154	–
2.2%Fe_2O_3/NaZSM-5	12.0	1.05	0.225	225		0.117	1.23
NaY	2.33	0.97	0	734	0.74	0.355	–
FeY(0.02)	2.34	0.63	0.095	691		0.336	0.89
FeY(0.1)	2.34	0.37	0.24	567		0.281	0.70
3.5%Fe_2O_3/NaY	2.33	0.97	0.095	636		0.317	1.35
8.6%Fe_2O_3NaY	2.33	0. 97	0.24	459		0.254	1.01

[a] Mole ratio of H_2 consumption during H_2-TPR to iron content.

Fe content usually resulted in a superior adsorption efficiency for ion-exchanged ferric zeolites (Table 2), while the impregnated samples present no less efficiency than their ion-exchanged analogs where 2.2%Fe_2O_3/NaZSM-5 and 8.6%Fe_2O_3/NaY, respectively exceed FeZ(0.02) and FeY(0.1) a lot.

Fig. 1 illustrates the TPSR profiles of NPYR on ferric zeolites, and the total amount of degraded NPYR is listed in Table 2. Judged from the amount of decomposed product NO_x, ion-exchanged FeZ samples were more active than parent NaZSM-5 (53.3 $\mu mol\ g^{-1}$) where FeZ(0.02) was better (121.0 $\mu mol\ g^{-1}$) than FeZ(0.1) (99.6 $\mu mol\ g^{-1}$). Differently, the NPYR degraded by FeY(0.1) (376 $\mu mol\ g^{-1}$) with higher ion-exchange extent was more than that by FeY(0.02) sample (335 $\mu mol\ g^{-1}$). All the impregnated ferric ZSM-5 and Y zeolites exhibited inferior capability to their ion-exchange analogs in NPYR degradation, and the Fe_2O_3/NaY was even weaker than its parent zeolite (Table 2). Besides, ion-exchanged ferric ZSM-5 could obviously lower the degrading temperature of NPYR down to the range of 453–533 K, while the impregnated 2.2%Fe_2O_3/NaZSM-5 sample maintained it (553–633 K) near to that of NaZSM-5 (533–613 K). FeZ(0.02) and 2.2%Fe_2O_3/NaZSM-5 have same Fe content, but the former is filtered and the latter is evaporated to keep its original sodium cations. For 2.2%Fe_2O_3/NaZSM-5 sample, some Na^+ ions would be exchanged by Fe guest when the zeolite contacted with $Fe(NO_3)_3$ solution, but these Fe^{3+} ions would be mostly driven away from cation sites by Na^+ in the evaporation step, forming Fe_2O_3 species outside the framework of zeolite after calcination, which is hard to improve the activity (Table 2). To check this inference, FeZ(0.02) was impregnated again with the solution containing extra added $NaNO_3$ which was equivalent to the Na^+ lost in previous ion-exchange, in order to examine whether these Na^+ ions substituted the Fe cations in the ferric zeolite. After calcination, the obtained sample denoted as Na-FeZ(0.02) was assessed in TPSR experiment. It could catalyze the decomposition in the range of 493–573 K and 90.7 $\mu mol\ g^{-1}$ of NPYR was degraded in the TPSR procedure, both situated between that of FeZ(0.02) and 2.2%Fe_2O_3/NaZSM-5. Since part of the Fe cation in ferric zeolite was exchanged by Na^+ so that the sample of Na-FeZ(0.02) became a composition of FeZ(0.02) and 2.2%Fe_2O_3/NaZSM-5 according to its catalytic performance. Introduction of Fe component to Y zeolite, either through ion-exchange or impregnation, brought an obvious improved activity in TPSR of NPYR with the degrading temperature decreasing from 593–613 K to 493–533 K (Fig. 1B). Likewise, more nitrosamines were degraded by the exchanged sample than impregnated analogs. Consequently, succeeding research was focused on these ferric Y zeolites.

Fig. 2 depicts the TPSR profiles of NNN, the representative of TSNA, on ferric zeolites. The degraded amount of NNN on these samples present the trend similar to that of NPYR: FeY(0.1) had the best performance (53.6 $\mu mol\ g^{-1}$), superior to FeY(0.02) (48.8 $\mu mol\ g^{-1}$) and parent NaY (39.1 $\mu mol\ g^{-1}$). 3.5%Fe_2O_3/NaY only decomposed 35.6 $\mu mol\ g^{-1}$ of NNN during TPSR procedure, again confirming the shortcoming of impregnated sample. Degrading temperature of NNN was also lowered from above 600 K (NaY) to 523–563 K. Their adsorption amounts of NNN seem a bit different from that of NPYR since NaY trapped more NNN (101.1 $\mu mol\ g^{-1}$) than its ferric analogs. Fig. S2A presents the TG results of NaY and ferric Y zeolites used in TPSR of NNN. Heavier coke formed in the ferric Y samples than parent NaY, and the coke amount was related to their catalytic activity, similar to that observed in zeolite HY [10]. Nonetheless, such coke formation contains the contribution of solvent dichloromethane adsorbed. For instance, FeY(0.1) adsorbed 0.09 $mmol\ g^{-1}$ of NNN (Table 2) whose molecular weight was 177 so the total weight of adsorbed NNN was about 1.6%; but the coke amount was estimated around 5%. As demonstrated in Fig. S2B, FeY(0.1) sample contacted with CH_2Cl_2 and experienced the same TPSR process also showed a coke amount of 3.9%.

Decomposition of NNN is also studied by TG-MS technique (Fig. 3), and the intensity of same compound released from different samples can be compared [28]. NO is known to be the primary product of nitrosamine degradation [29], Fig. 3A showed the intensity of NO (m/z = 30) signal on ferric Y zeolites. The Fe species on zeolite not only increased the amount of released NO but also lowered the degrading temperature of NNN, especially on the ion-exchanged sample. N_2O (m/z = 44, Fig. 3B) is another degradation product of nitrosamines formed by disproportionation of $3NO \rightarrow N_2O + NO_2$ [24], so that N_2O signal appeared in the higher temperature region

Table 2
TPSR results of ferric zeolites and their parents.

Sample	Total NPYR adsorbed ($\mu mol\ g^{-1}$)	NPYR adsorbed in unit area ($\mu mol\ m^{-2}$)	NPYR degraded ($\mu mol\ g^{-1}$)	Total NNN adsorbed ($\mu mol\ g^{-1}$)	NNN adsorbed in unit area ($\mu mol\ m^{-2}$)	NNN degraded ($\mu mol\ g^{-1}$)
NaZSM-5	375.3	1.23	53.3	–	–	–
FeZ(0.02)	396.2	1.21	121.0	–	–	–
FeZ(0.1)	389.4	1.40	99.6	–	–	–
2.2%Fe_2O_3/NaZSM-5	362.8	1.61	63.0	–	–	–
NaY	407.9	0.56	238.4	101.1	0.138	39.1
FeY(0.02)	462.5	0.67	335.4	89.6	0.130	48.8
FeY(0.1)	425.8	0.75	376.2	94.1	0.166	53.6
3.5%Fe_2O_3/NaY	427.0	0.67	162.0	91.7	0.144	35.6
8.6%Fe_2O_3/NaY	412.9	0.90	163.6	–	–	–

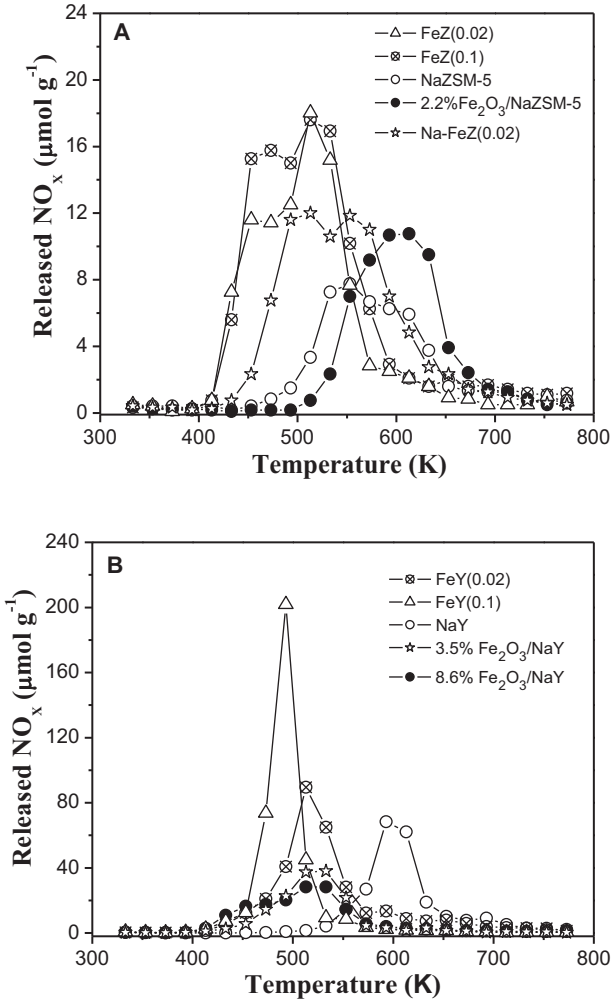

Fig. 1. The NO_x detected in the temperature programmed surface reaction (TPSR) of NPYR on ferric zeolites and their parents.

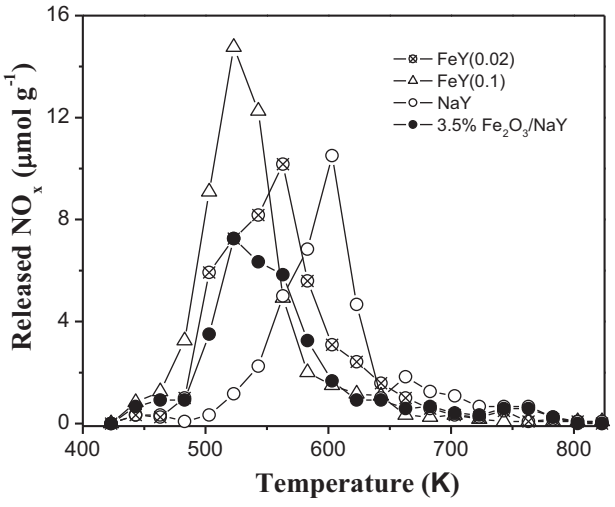

Fig. 2. The NO_x detected in the temperature programmed surface reaction (TPSR) of NNN on NaY and ferric Y samples.

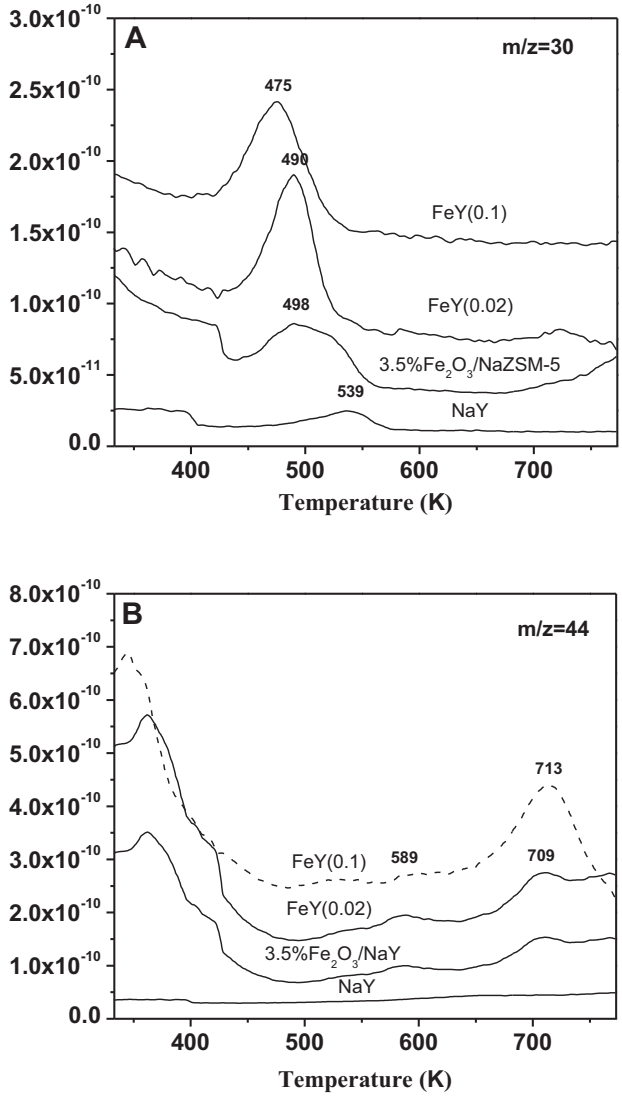

Fig. 3. The MS signals of decomposed products of NNN desorbed from NaY and ferric Y samples during the TPSR procedure (The ion current for 3.5%Fe_2O_3/NaZSM5, FeY(0.02) and FeY(0.1) are offset vertically by 3×10^{-11}, 6×10^{-11}, 12×10^{-11} in Fig. 4A and 3×10^{-11}, 10×10^{-11}, 20×10^{-11} in Fig. 4B, respectively).

than that of NO. Much more N_2O was detected on ferric Y samples than that on NaY, but the distinction between ferric Y zeolites was unconspicuous.

3.3. Analysis of Fe state on the ferric zeolites

Fig. S3 depicts the UV–vis diffuse-reflectance spectra (DRS) of ferric zeolites. The absorbance lower than the wavelength of 270 nm is attributed to ligand-to-metal charge transfer, while the bands higher than 270 nm are assigned to ligand field (d–d) transitions and pair excitations processes of magnetically coupled Fe^{3+} cations [30,31]. Consequently, the absorbance at about 220 and 270 nm corresponds to isolated Fe^{3+} species whereas those between 300 and 400 nm are assigned to cluster Fe-species including dimeric or oligomeric species [32–34]; and absorbance higher than 400 nm is related to Fe_2O_3 particles outside zeolite framework [32,33]. The relative concentrations of various Fe species formed on zeolite are estimated in Table S1. All ferric zeolites had absorbance bands at 300–600 nm more or less, indicating somewhat of Fe cluster or oxide species formation at this

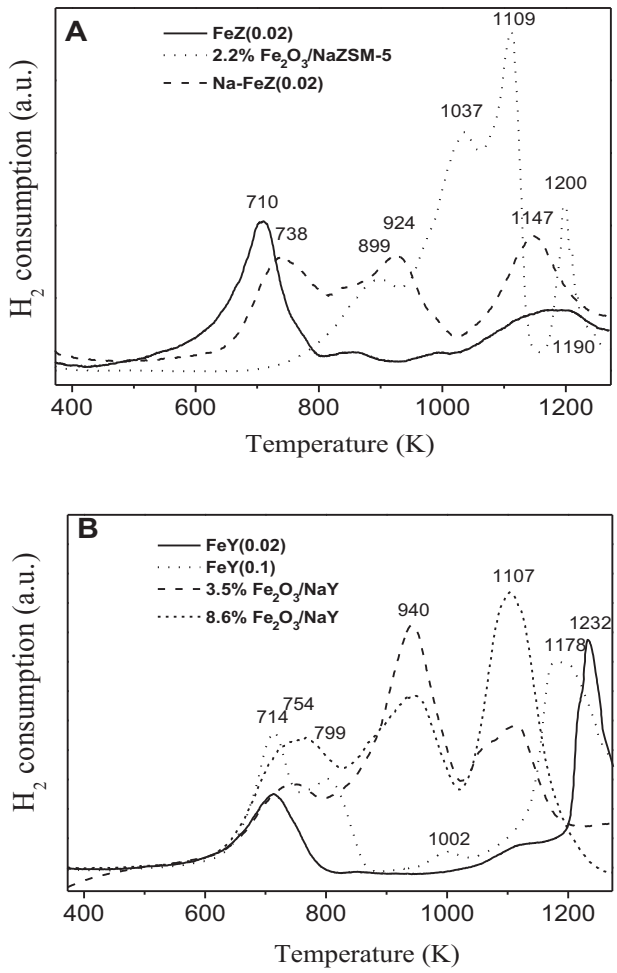

Fig. 4. H_2-TPR profiles of ferric zeolite samples.

level of Fe content [35]. The band intensity at 400–600 nm followed the order of 2.2%Fe_2O_3/NaZSM-5 > FeZ(0.1) > FeZ(0.02) and 8.6%Fe_2O_3/NaY > FeY(0.1) > 3.5%Fe_2O_3/NaY > FeY(0.02), paralleling to the decrement of surface area and pore volume of these samples (Table 1). Fe_2O_3 species was easier to be formed on the sample prepared by impregnation than ion-exchange, and higher concentration of ion-exchange solution led to more Fe aggregation species.

H_2-TPR profiles of ferric zeolites are shown in Fig. 4. The reduction of Fe species on ion-exchanged FeZ(0.02) sample mostly occurred in two stages. The first peak at 710 K was the reduction of Fe^{3+} to Fe^{2+}, and the second broad peak around 1190 K was assigned to the reduction of Fe^{2+} to Fe^0 [14,15]. 2.2%Fe_2O_3/NaZSM-5 sample had a completely different profile. It showed three peaks between 800–1150 K, corresponded to the reduction of Fe_2O_3 to Fe_3O_4, Fe_3O_4 to FeO and FeO to Fe^0, respectively [13,36], and the reduction of Fe oxide on this sample shifts to a higher temperature in comparison with pure Fe_2O_3 (Fig. S4). There was a small peak at 1200 K on this sample which is attributed to the reduction of Fe^{2+} cations to Fe^0, indicating the existence of small amount of Fe^{3+} cations in the impregnated samples, which was in line with the UV–vis DRS result. For the Na-FeZ(0.02) sample, the first broad peak around 738 K stood for the reduction of Fe^{3+} cations to Fe^{2+}; the second peak (800–1000 K) was attributed to the reduction of Fe oxide species [15] while the last one at 1147 K represented the reduction of Fe^{2+} cations to Fe^0. The Fe species on Na-FeZ(0.02) shows a composited state of that on FeZ(0.02) and 2.2%Fe_2O_3/NaZSM-5. For ferric Y zeolites, obvious distinction was observed between the ion-exchanged and impregnated samples: 3.5%Fe_2O_3/NaY and 8.6%Fe_2O_3/NaY showed two large peaks of H_2 consumption at 940 and 1100 K, corresponding to the two reduction peaks of Fe_2O_3 (Fig. S4) but also shifting to a higher temperature like on ZSM-5 matrix. Whereas, the H_2 consumption around 750 K on them revealed somewhat of ion-exchange occurred during impregnation. On the other hand, the reduction peaks of e FeY(0.02) and FeY(0.1) emerged at 700 K and 1200 K which stood for the process of Fe^{3+} to Fe^{2+} and Fe^{2+} to Fe^0, respectively [37]. The small peaks at 800 K and 1000 K on FeY(0.1) illustrated slight formation of Fe_2O_3 oxide species [19]. The H_2/Fe molar ratio yielded from the area of TPR peaks are listed in Table 1, where all the sample had the ratio more than 0.5 but less than 1.5, mirroring that Fe(III) was reduced to lower valence than 2 but far from completely reduction to Fe^0. The extent of reduction on ion-exchanged samples was relatively small because the reduction of Fe^{2+} to Fe^0 needs the collapse of zeolite framework [37]. Fe oxide species on impregnated sample was much easier to be reduced, resulting in a bit higher H_2/Fe ratio. As the Fe content increased, the reduction extent decreased both for ion-exchanged and impregnated samples.

3.4. Selective reduction of TSNA in smoke

Table 3 shows the performance of ferric zeolites to reduce TSNA content in the mainstream smoke of Burley type cigarette. We utilize the TSNA/TPM ratio to eliminate the system error caused in smoking procedure [8]; and this value demonstrates the TSNA content in unit TPM, reflecting the selective reduction of TSNA from particulate matter in smoke. Both NaZSM-5 and NaY zeolite could selectively reduce about 15% of TSNA in smoke; and ion-exchanged ferric zeolites increased the removal from 15% to 20–26% (Table 3) except for FeZ(0.1) whose activity was almost unchanged. However, the impregnated ferric ZSM-5 and Y zeolites showed lower activities and their selective removal of TSNA decreased to 8–9%. FeY(0.1) was the best sample among these cig-cat additives and could selectively remove 26% of TSNA in smoke. Moreover, it still had a considerable activity to selectively remove TSNA in smoke (18.0%) after stored for 2 months.

Table S2 displays the selective reduction of four TSNA components by ferric zeolite. Among these four components, NAB was quite less than others so that we focused on other three components, NNN, NNK and NAT. No preference was observed on NaZSM-5 and NaY, but ion-exchanged ferric zeolites had the orderliness of NNN > NNK > NAT (Table S2). For the impregnated samples, however, both reduction ratio of NNN and NAT were quite inferior to that of NNK. Fe_2O_3 species has special affinity to NNK, so the ratio of removed NNK by FeZ(0.1) and FeY(0.1) were higher than that by FeZ(0.02) and FeY(0.02) because the former two had a little bit of Fe_2O_3 species as aforementioned. Storage of two months lowered the catalytic activity of FeY(0.1), but the reduction of TSNA still followed the order of NNN > NNK > NAT (Table S2).

Fig. 5 depicts the proportion of nitrosamine degraded in TPSR procedure and the selective reduction of TSNA in smoke by zeolites. The high catalytic activity of zeolite in TPSR procedure indicates its high ability to cleavage the N—NO group of nitrosamine [3,9], and such cleavage is necessary for degradation of TSNA [4,23]. The degraded proportion of different nitrosamines (NPYR and NNN) on ferric Y zeolites followed the same trend, that is, FeY(0.1) > FeY(0.02) > NaY > 3.5%Fe_2O_3/NaY (Fig. 5B). As a result, the sample with higher activity to degrade nitrosamine in TPSR experiment also exhibited better performance in selectively removing TSNA in tobacco smoke.

Table 3
TSNA content and related data of smoking experiment on Burley type cigarette with addition of zeolites.

Sample	Weight of cigarette (mg cig^{-1})	Pressure drop (Pa)	TPM (mg cig^{-1})	Reduction of TPM (%)	TSNA (ng cig^{-1})	TSNA/TPM (ng mg^{-1})	Selective reduction of TSNA (%)
NaZSM-5	934	1278	14.0	0.7	120.0	8.57	15.4
FeZ(0.02)	913	1250	14.9	−5.7	120.2	8.07	20.3
FeZ(0.1)	925	1310	14.9	−5.7	129.0	8.65	14.6
2.2%Fe_2O_3/NaZSM-5	943	1275	14.6	−3.5	135.5	9.28	8.4
NaY	929	1293	12.5	11.3	108.3	8.66	14.5
FeY(0.02)	927	1334	14.6	−3.5	115.4	7.90	22.0
FeY(0.1)	939	1259	13.4	5.0	100.0	7.46	26.4
3.5%Fe_2O_3/NaY	925	1232	12.0	14.9	109.8	9.15	9.7
FeY(0.1)[a]	939	1292	13.3	5.7	110.6	8.31	18.0
Blank	916	1175	14.1	–	142.9	10.13	–

[a] The data was collected after treated cigarettes storing at 277 K for two months.

4. Discussion

According to H_2-TPR results, there were various states of Fe on ferric zeolites (Fig. 4), namely the Fe^{3+} in cation site and aggregated Fe_2O_3 particles dispersed in zeolite. The Fe_2O_3 species on zeolite have minor contribution to the catalytic degradation of nitrosamine, and some impregnated ferric zeolites degraded even less nitrosamine than their parents in TPSR experiment (Table 2, Figs. 1 and 2). Thus, the main ferric active species in zeolite should be the exchanged cation and dimer or oligomer species inside the channel. They strengthen the affinity toward nitrosamine and induce it to be adsorbed and then catalyzed the rupture of N—NO bond to degrade this carcinogen [9,23].

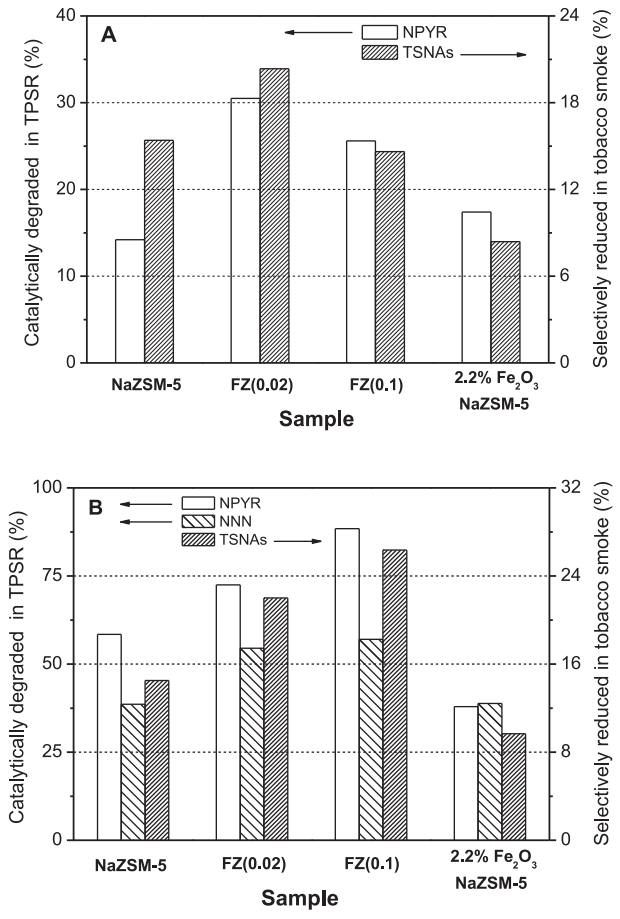

Fig. 5. The proportion of nitrosamines degraded in TPSR procedure and the selective reduction of TSNA in tobacco smoke by ferric zeolites and their parents.

Ion exchange ensures iron ions locate in the framework of zeolite. Although the ion-exchange of zeolite simultaneously happens once zeolite is put into the impregnation solution [14], those Na^+ ions which have been exchanged will gradually occupy the cation sites again during the evaporation of water in impregnation, and drive most of exchanged Fe^{3+} out of framework. These re-exchanged Fe^{3+} cations finally converted to Fe_2O_3 nanoparticles. Due to the different distribution of ferric species, FeZ(0.02) exhibited a higher catalytic activity in TPSR test of NPYR than 2.2%Fe_2O_3/NaZSM-5 (Fig. 1A). When FeZ(0.02) sample was impregnated by $NaNO_3$ solution whose amount was equivalent to the Na^+ lost in previous exchange, the resulting sample Na-FeZ(0.02) had a lower activity than FeZ(0.02), because some iron ions were re-exchanged out of framework; consequently, it had the special features between that of FeZ(0.02) and 2.2%Fe_2O_3/NaZSM-5 (Figs. 1A and 2). Na-FeZ(0.02) and 2.2%Fe_2O_3/NaZSM-5 samples had the same chemical composition, but different preparation changed their distribution of Fe species, resulting in different catalytic performance in TPSR test (Fig. 1A).

The TSNA species in smoke are blended with many other compounds to form micrometer particles [11,12]. When the cigarette is puffed, these particles flow with mainstream smoke and continually collide with posterior unburned tobacco, inevitably contacting with the zeolite in tobacco rods. These zeolite additives would interact with TSNA located on the surface of particles through special electrostatic interaction [6], adsorbing them followed by the catalytic degradation at high temperature of combustion (Scheme 1, take NNN as a representative). Two inherent features of zeolite, geometric confinement and electrostatic attraction [23,38], enable the degradation of TSNA to be realized. Nitrosamine has the functional group of N—NO whose oxygen atom possesses negative charge, so the nitrosamine molecule is strongly attracted by the cations in zeolite framework. When the nitrosamine molecule is close to the pore mouth of zeolite, it is instantaneously adsorbed due to the interaction between their N—NO group and the cations in zeolite [3,4,6]. The bulky TSNA molecule will insert its N-NO group into the channel of zeolite [23], and the thermal movement of the rest part of NNN molecule will lead to break of the N—N bond at elevated temperature [38]. Compared with Na^+ ion in zeolite, Fe^{3+} cation has a stronger attraction toward nitrosamine. Since the iron in ion-exchanged ferric zeolite always present in the octahedral Fe^{3+} ions [30] (which have 5d-electrons) may offer two empty e_g orbitals to the N—NO group only in the 'low spin' configuration (all five electrons occupying the three t_{2g} orbitals), the N—NO group could strongly interact with the empty 3d orbitals of the Fe^{3+} cations; however, for the more common high spin configuration of Fe^{3+} species (all five d-orbitals singly occupied), the cleavage of the N—NO bonds may be favored by the radical intermediates, or radical adducts resulting from the photolysis or pyrolysis of nitrosamines [39] which in some way might strongly interact with the two singly

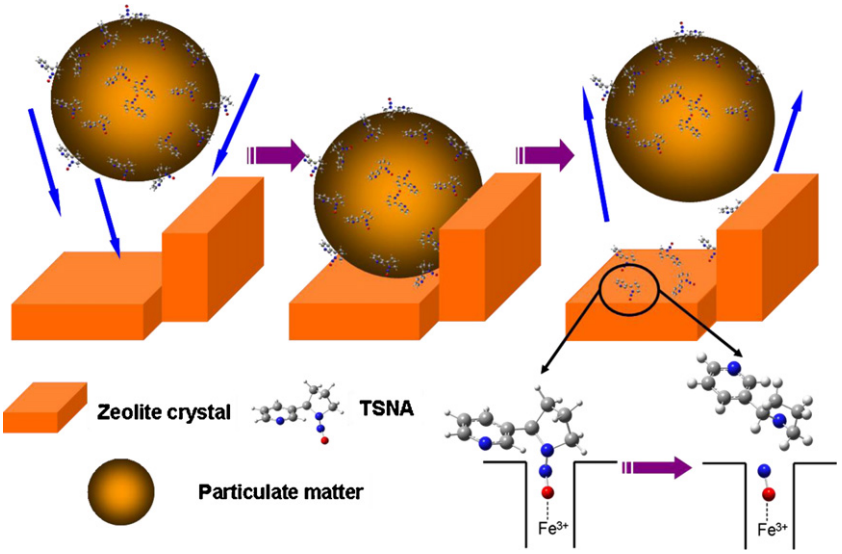

Scheme 1. The mechanism of action on removing TSNA from particulate matter in smoke by ferric zeolite.

occupied e_g orbitals of the Fe^{3+} ions. Consequently, the Fe^{3+} cations inside the zeolite framework show high efficiency to catalytically degrade the nitrosamines with synergy of the geometric confinement provided by the microchannel. Contrarily, for Fe_2O_3 particles outside zeolite framework, the 3d orbitals of Fe(III) would not be any longer available because it is replaced by the typical band structure of the oxides. As a result, the impregnated samples are inferior in catalytic degradation because of their weaker interaction to nitrosamines as well as the absence of assistance of microchannel.

The function of zeolite is limited in the system with complex chemical composition. In laboratory adsorption of volatile nitrosamine such as NPYR, both NaY and NaZSM-5 zeolites could capture almost all of the carcinogens when 0.2 mmol g^{-1} of NPYR passed at 593 K [40]. Nonetheless, they trapped only 1.37 and 1.11 μmol g^{-1} of TSNA, respectively, in the tobacco-extract aqueous solution [41]. And the situation is worse for them in tobacco smoke to remove the TSNA. It is the nightmare of catalyst because tobacco smoke consists of thousands of compounds [5,11] and the contact time of catalyst to targets is also less than 0.1 s [8]. Most TSNA exist in the particulate matter of smoke and these particles have average size of micrometer [7], and only the TSNA on the surface of the particles can be captured by zeolite. These difficulties make the *in situ* removal of TSNA in tobacco smoke much more difficult than that in ordinary laboratory test. Present results offer a clue to control the pollution caused by smoking. Ferric zeolites, especially the FeY(0.1) sample, give promising data that about quarter of TSNA can be *in situ* eliminated selectively from the particulate matter of smoke (Table 3). Moreover, the selective reduction of TSNA in tobacco smoke by zeolite follows the trend of catalytic ability in decomposing nitrosamine in TPSR test (Fig. 5). Thus, TPSR test can be used for preliminary screening cig-cat candidates in order to seek new efficient catalyst for eliminating TSNA pollutants.

5. Conclusion

Some conclusive remarks can be tentatively derived from the results mentioned above,

(1) Ion exchanged ferric zeolite shows a higher activity of degrading nitrosamines than its impregnated analog in both TPSR test and l smoke, indicating the Fe cations in zeolite framework are better than Fe_2O_3 nanoparticles in catalyzing the decomposition of nitrosamines.
(2) Ferric zeolites added to the tobacco rods of cigarette can selectively reduce at most 26% of TSNA from the particulate matter in mainstream smoke for Burley type tobacco; and the catalyst remains valid after storage for two months.
(3) Cleavage of N—NO bond in nitrosamine molecule is the key step of nitrosamine degradation in both simple and complex conditions. The performance of selectively removing TSNA in smoke by zeolites parallels their degradation abilities of nitrosamines in TPSR test.

Acknowledgments

Financial support from NSF of China (20873059, 21173117 and 21273106), the Scientific Research Foundation of Graduate School and the Analysis Centre of Nanjing University is gratefully acknowledged.

Appendix A. Supplementary data

Supplementary data associated with this article can be found, in the online version, at http://dx.doi.org/10.1016/j.apcatb.2012.09.039.

References

[1] S.S. Hecht, Mutation Research 424 (1999) 127–142.
[2] K. Hiramoto, T. Ohkawa, K. Kikugawa, Free Radical Research 35 (2001) 803–813.
[3] Y. Xu, H.D. Liu, J.H. Zhu, Z.Y. Yun, J.H. Xu, Y.L. Wei, New Journal of Chemistry 28 (2004) 244–252.
[4] C.F. Zhou, Y.M. Wang, Y. Cao, T.T. Zhuang, W. Huang, Y. Chun, J.H. Zhu, Journal of Materials Chemistry 16 (2006) 1520–1528.
[5] W.M. Meier, K. Siegmann, Microporous and Mesoporous Materials 33 (1999) 307–310.
[6] L. Gao, Y. Wang, Y. Xu, S.L. Zhou, T.T. Zhuang, Z.Y. Wu, J.H. Zhu, Clean: Soil, Air, Water 36 (2008) 270–278.
[7] Y. Zhou, L. Gao, F.N. Gu, J.Y. Yang, J. Yang, F. Wei, Y. Wang, J.H. Zhu, Chemistry: A European Journal 15 (2009) 6748–6757.
[8] L. Gao, Y. Cao, S.L. Zhou, T.T. Zhuang, Y. Wang, J.H. Zhu, Journal of Hazardous Materials 169 (2009) 1034–1039.
[9] Z.Y. Wu, H.J. Wang, L.L. Ma, J. Xue, J.H. Zhu, Microporous and Mesoporous Materials 109 (2008) 436–444.
[10] Y. Cao, T.T. Zhuang, J. Yang, H.D. Liu, W. Huang, J.H. Zhu, Journal of Physical Chemistry C 111 (2007) 538–548.
[11] R.R. Baker, in: D.L. Davis, M.T. Nielsen (Eds.), Tobacco Production, Chemistry and Technology, Blackwell, Oxford, 1999, pp. 419–427.
[12] C.H. Keith, Beitr Tabakforsch International 11 (1982) 123–131.

[13] H.Y. Chen, W.M.H. Sachtler, Catalysis Today 42 (1998) 73–83.
[14] A. Guzmán-Vargas, G. Delahay, B. Coq, Applied Catalysis B: Environmental 42 (2003) 369–379.
[15] K. Krishna, G.B.F. Seijger, C.M. van den Bleek, M. Makkee, G. Mul, H.P.A. Calis, Catalysis Letters 86 (2003) 121–131.
[16] S. Brandenberger, O. Kröcher, M. Casapu, A. Tissler, R. Althoff, Applied Catalysis B: Environmental 101 (2011) 549–659.
[17] G. Qi, J.E. Gatt, R.T. Yang, Journal of Catalysis 226 (2004) 120–128.
[18] K. Jíša, J. Nováková, M. Schwarze, A. Vondrová, S. Sklenák, Z. Sobalik, Journal of Catalysis 262 (2009) 27–34.
[19] A.C. Akah, G. Nkeng, A.A. Garforth, Applied Catalysis B: Environmental 74 (2007) 34–39.
[20] K.A. Wagner, N.H. Finkel, J.E. Fossett, I.G. Gillman, Analytical Chemistry 77 (2005) 1001–1006.
[21] R. Schmidt, M.D. Amiridis, J.A. Dumesic, Journal of Physical Chemistry 96 (1992) 8142–8149.
[22] T. Nobukawa, K. Sugawara, K. Okumura, Applied Catalysis B: Environmental 70 (2007) 342–352.
[23] Y. Cao, Z.Y. Yun, J. Yang, X. Dong, C.F. Zhou, T.T. Zhuang, Q. Yu, H.D. Liu, J.H. Zhu, Microporous and Mesoporous Materials 103 (2007) 352–362.
[24] J.Y. Yang, Q. Hou, F. Wei, W.G. Lin, F.N. Gu, Y. Zhou, J.H. Zhu, Chemical Engineering Journal 169 (2011) 390–398.
[25] M. Schwidder, M.S. Kumar, K. Klementiev, M.M. Phol, A. Brückner, W. Grünert, Journal of Catalysis 231 (2005) 314–330.
[26] M.S. Batista, M.A. Morales, E. Baggio-Saitovich, E.A. Urquieta-Gonzalez, Hyperfine Interactions 134 (2001) 161–166.
[27] M. Dükkancı, G. Gündüz, S. Yılmaz, Y.C. Yaman, R.V. Prikhod'ko, I.V. Stolyarova, Applied Catalysis B: Environmental 95 (2010) 270–278.
[28] T. Rudolf, A. Pöppl, W. Brunner, D. Michel, Magnetic Resonance in Chemistry 37 (1999) S93–S99.
[29] J.P. Cheng, M. Xian, K. Wang, X. Zhu, Z. Yin, P.G. Wang, Journal of the American Chemical Society 120 (1998) 10266–10267.
[30] G. Fierro, G. Moretti, G. Ferraris, G.G. Andreozzi, Applied Catalysis B: Environmental 102 (2011) 215–223.
[31] D.M. Sherman, T.D. Waite, American Mineralogist 70 (1985) 1262–1269.
[32] M.S. Kumar, M. Schwidder, W. Grünert, A. Brückner, Journal of Catalysis 227 (2004) 384–397.
[33] S. Bordiga, R. Buzzoni, F. Geobaldo, C. Lamberti, E. Giamello, A. Zecchina, G. Leofanti, G. Petrini, G. Tozzola, G. Vlaic, Journal of Catalysis 158 (1996) 486–501.
[34] J. Perez-Ramirez, M.S. Kumar, A. Bruckner, Journal of Catalysis 223 (2004) 13–27.
[35] S. Brandenberger, O. Kröcher, A. Tissler, R. Althoff, Applied Catalysis A: General 373 (2010) 168–175.
[36] L.J. Lobree, I.-C. Hwang, J.A. Reimer, A.T. Bell, Journal of Catalysis 186 (1999) 242–253.
[37] L. Li, Q. Shen, J. Li, Z. Hao, Z.P. Xu, G.Q. Max Lu, Applied Catalysis A: General 344 (2008) 131–141.
[38] J. Yang, Y. Zhou, H.J. Wang, T.T. Zhuang, Y. Cao, Z.Y. Yun, Q. Yu, J.H. Zhu, Journal of Physical Chemistry C 112 (2008) 6740–6748.
[39] T.A. Grover, J.A. Ramseyer, L.H. Piette, Free Radical Biology and Medicine 3 (1987) 27–32.
[40] C.F. Zhou, Y. Cao, T.T. Zhuang, W. Huang, J.H. Zhu, Journal of Physical Chemistry C 111 (2007) 4347–4357.
[41] F. Wei, F.N. Gu, Y. Zhou, L. Gao, J. Yang, J.H. Zhu, Solid State Sciences 11 (2009) 402–410.